
This is an electronic reprint of the original article.
This reprint may differ from the original in pagination and typographic detail.

Tzarouchis, Dimitrios C.; Ylä-Oijala, Pasi; Sihvola, Ari
Study of Plasmonic Resonances on Platonic Solids

Published in:
Radio Science

DOI:
[10.1002/2017RS006378](https://doi.org/10.1002/2017RS006378)

Published: 01/12/2017

Document Version
Publisher's PDF, also known as Version of record

Please cite the original version:
Tzarouchis, D. C., Ylä-Oijala, P., & Sihvola, A. (2017). Study of Plasmonic Resonances on Platonic Solids. *Radio Science*, 52(12), 1450–1457. <https://doi.org/10.1002/2017RS006378>

This material is protected by copyright and other intellectual property rights, and duplication or sale of all or part of any of the repository collections is not permitted, except that material may be duplicated by you for your research use or educational purposes in electronic or print form. You must obtain permission for any other use. Electronic or print copies may not be offered, whether for sale or otherwise to anyone who is not an authorised user.



RESEARCH ARTICLE

10.1002/2017RS006378

Key Points:

- The main geometrical features of the Platonic solids and their plasmonic responses are discussed
- Strong correlation is found between the shift of the dipole plasmon resonance and the sharpness of vertex angle of the solid
- Albedo spectra reveal individual signatures of different Platonic solids

Correspondence to:

D. C. Tzarouchis,
dimitrios.tzarouchis@aalto.fi

Citation:

Tzarouchis, D. C., Ylä-Oijala, P., & Sihvola, A. (2017). Study of plasmonic resonances on Platonic solids. *Radio Science*, 52. <https://doi.org/10.1002/2017RS006378>

Received 30 MAY 2017

Accepted 24 OCT 2017

Accepted article online 28 OCT 2017

Study of Plasmonic Resonances on Platonic Solids

Dimitrios C. Tzarouchis¹ , Pasi Ylä-Oijala¹, and Ari Sihvola¹

¹Department of Electronics and Nanoengineering, School of Electrical Engineering, Aalto University, Espoo, Finland

Abstract In this study we discuss the plasmonic subwavelength scattering resonances of five regular polyhedra, that is, the Platonic solids tetrahedron, hexahedron, octahedron, dodecahedron, and icosahedron. A brief discussion regarding their geometrical characteristics and the numerical method used in the study is given. All results are compared with the benchmark case of a sphere, in order to observe how the geometry of the solid affects the spectral characteristics. The principal finding is that the shift of the main dipole resonance exhibits a solid vertex hierarchical order; in other words, the position of the resonance correlates with the solid angle of the vertex of the given solid. This is in contrast with the hedra-hierarchical order found for the electrostatic dielectric response of these solids. These results can create new avenues for applications and devices that require plasmonic particles with on-demand functionalities.

1. Introduction

The optical properties of nanoparticles (NP) have generated increasing research interest due to the recent advances in nanotechnology. A particularly interesting case of NP are the plasmonic NPs (Lagos et al., 2017; Mitiche et al., 2017), that is, particles able to support localized charge oscillations, also known as localized surface plasmons Quinten (2010). These resonances are affected by the specific geometrical and material characteristics, widely used for radiation control and harvesting applications (Akselrod et al., 2014; Yang et al., 2017).

In this work the scattering spectrum of plasmonic Platonic solids is numerically investigated. The presented results are extension of the results (Tzarouchis et al., 2016) presented in the 2016 URSI Electromagnetic Theory Symposium, Aalto University, Espoo, Finland. There the resonant plasmonic spectrum of rounded hexahedra and octahedra was numerically evaluated using a surface integral equation technique. Here we extend these results by including and discussing the plasmonic resonances of the whole family of the Platonic solids. Platonic solids are a particular case of regular polyhedra that attract the theoretical and experimental interest regarding their scattering characteristics (Kim et al., 2004; Ringe et al., 2012; Ross et al., 2015; Sihvola et al., 2004).

This article is divided into three parts. First, in section 2 the main material characteristics, the geometrical features of the Platonic solids, and the numerical method used are given. Section 3 presents the main results for each of the solids, with the spectrum of an equivolumed sphere given as benchmark. Section 4 concludes the discussion by presenting some comparative results between the five polyhedra and an equivolumed spherical nanoparticle.

2. Problem Preliminaries

The main objective of this work is the study of the resonant plasmonic behavior of subwavelength nanoparticles. Localized surface plasmon resonances (LSPR or plasmonic resonances) are a particular type of discrete resonances naturally occurring for metals in the infrared (IR)-optical-ultraviolet (UV) region. These resonances are due to the collective oscillations of the free conduction electrons in metals (incompressible plasma gas). This plasma response can be macroscopically described through various material dispersion models, such as the Drude model, where the material permittivity results as a damped oscillation over a certain central frequency (plasma frequency) and a certain amount of oscillation losses (damping frequency).

In our case all NPs are modeled with a simple, Drude-like model for silver (Ag), that is,

$$\epsilon_{Ag}(\lambda) = \epsilon_{\infty} + \frac{(\lambda/\lambda_p)^2}{1 - j\lambda/\lambda_d}, \quad (1)$$

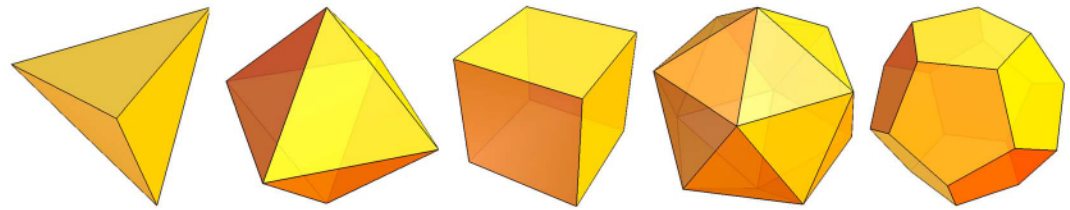


Figure 1. The five Platonic solids (regular polyhedra) presented in a solid vertex hierarchical order. From left to right: tetrahedron, octahedron, hexahedron (cube), icosahedron, and dodecahedron with 4, 8, 6, 20, and 12 edges, respectively. The sv-hierarchy is visible in the increasing smoothness of the shapes from left to right.

where $\epsilon_\infty = 5.5$, $\lambda_p = 130$ nm, and $\lambda_d = 30$ μ m, introduced in (Wallén et al., 2009). This model is a curve fit on Johnson and Christy (1972) experimental data for bulk silver. Silver is a widely used reference material, mostly due to its strong plasmonic resonances occurring at the optical-near UV spectrum (Kreibig & Vollmer, 2013). Since the used model is a simple Drude model, all of the presented results can be qualitatively expanded covering other types of materials modeled by a Drude model, such as gold (Au) and aluminum (Al) (Palik, 1998).

As a remark, the optical response of small particles is expected to be slightly different from the bulk limit (Kreibig, 1974), in particular, with respect to the losses. Our analysis concentrates in exploring and comparing the general behavior of the main plasmonic resonances in the regime where these size-dependent effects can be neglected, and a simple Ag-Drude model experiencing low-to-moderate level of dissipative losses is valid. Note that the volume of each of the NPs considered in this paper is 50^3 nm³.

2.1. Geometrical Features of Platonic Solids

Although there are infinite regular polygons in two dimensions, in three-dimensional space there are only five (Figure 1), that is, the tetrahedron, octahedron, hexahedron (cube), icosahedron, and dodecahedron, commonly recognized as the Platonic solids (these five solids play an instrumental role in Plato’s natural philosophy Weyl, 2015). From a physical point of view these structures occur either naturally in organic and inorganic compounds or artificially engineered NPs. Some of the geometrical properties of these solids are given in Table 1 where we can find the volume and vertex solid angle for each solid. One interesting property is the duality between these solids. For instance, a hexahedron can be transformed to an octahedron by mutually interchanging the number of faces and number of vertices (see Figure 1 and Table 1). The same applies for dodecahedron and icosahedron while tetrahedron is self-dual. These duality relations are a key issue in understanding and categorizing the plasmonic behavior of the solids.

Classically, the preferred order for categorizing the Platonic solids is by the number of the edges, that is, the order tetra-hexa-octa-dodeca-icosa, implies the ascending number of faces (hedra) of each solid. We name this as the *hedra-hierarchical* order, or h-hierarchy for short. However, instead of the h-hierarchy there is another way of categorization following the *sharpness* of a solid, that is, based on its solid angle vertex. This categorization results in the tetra-octa-hexa-icosa-dodeca scheme, and we call it *solid vertex* hierarchy, or sv-hierarchy for short. In this work we adopt an sv-hierarchical order for presenting the results for each NP.

Hence, the analysis will start with a smooth sphere and will follow the sv-hierarchical order, that is, dodeca-icosa-hexa-octa-tetra, as can be seen in the next sections.

2.2. Surface Integral Equation Method

In the numerical analysis of this article, all the necessary field and scattering quantities of the Platonic solids are computed with the surface integral equation (SIE) method. This widely used method offers accurate and reliable solutions for many computational electromagnetics problems, a review of which is given by Ylä-Oijala et al. (2014). The SIE methods has been recently extended for the modeling of plasmonic scatterers and nanoantennas, by García de Abajo and Howie (2002), Hohenester and Krenn (2005), Kern and Martin (2009), Taboada et al. (2011), Solis et al. (2015), and others.

The SIE method is based on Love’s equivalence principle, allowing the reformulation of the original problem of solving Maxwell’s equations in the entire

Table 1
Key Features of the Platonic Solids

Polyhedron	Volume	Vertex angle (rad) \approx	Edge ³ a (nm)
Tetrahedron	$\frac{\sqrt{2}}{12}a^3$	0.551	101.98
Octahedron	$\frac{\sqrt{2}}{3}a^3$	1.359	64.245
Hexahedron	a^3	$\frac{\pi}{2} = 1.571$	50
Icosahedron	$5\frac{3+\sqrt{5}}{12}a^3$	2.635	38.55
Dodecahedron	$\frac{15+7\sqrt{5}}{4}a^3$	2.962	25.36

Note. All solids are adjusted to have the same volume.

^aRequired edges for equivolumented particles.

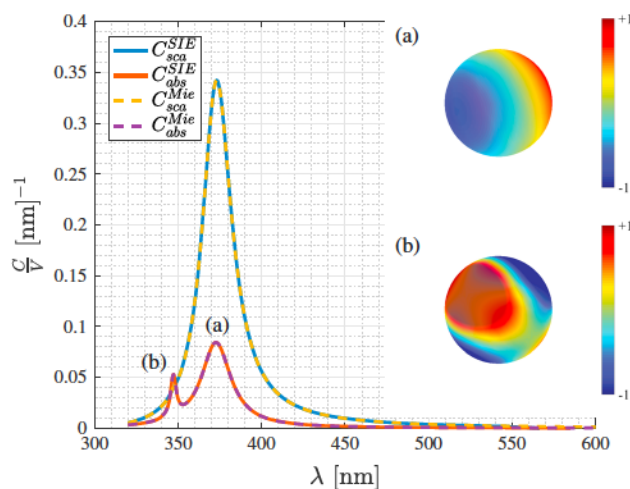


Figure 2. The volume-normalized ($V=50^3 \text{ nm}^3$) scattering and absorption spectra for a sphere of diameter $d=62.035 \text{ nm}$ extracted both analytically using the Lorenz-Mie theory (Bohren & Huffman, 2008) (dashed lines) and SIE method (solid lines). The inset figures depict the normalized surface charge distribution for (a) the imaginary part of charge distribution at $\lambda=372.7 \text{ nm}$ (electric dipole) and (b) the real part of the charge distribution at $\lambda=347.1 \text{ nm}$ (electric quadrupole). The charge normalization is in arbitrary units for better visibility of the results.

3-D space as an equivalent problem of solving equivalent sources (currents) on the surfaces and interfaces. This numerical method is thus especially well suited for modeling LSPR, where most of the physical phenomena take place on the surfaces. Many other numerical treatments of plasmonic nanoparticles can be found based on a volume-oriented philosophy, such as the Discrete dipole approximation (DDA) (Grillet et al., 2011; Noguez, 2007), the volume boundary element method (BEM-3D) (García de Abajo & Howie, 2002), and the finite element method (FEM) (Grillet et al., 2011). All of the aforementioned methods are appealing for certain applications, demonstrating strengths and weaknesses regarding the proper evaluation of the required quantities. In other words, the proper choice of a numerical method should be always aligned with the specific simulation needs. For instance, as has been showed recently by Vartia et al. (2016), SIE can outperform DDA in certain near field characteristics of small NPs.

The method used here is based on the classical PMCHWT integral equation formulation described in detail by (Ylä-Oijala et al., 2005). In brief, in that method Love's equivalence principle is applied in each homogeneous and isotropic region. Then by enforcing the tangential continuity of the electromagnetic fields, a set of coupled surface integral equation is obtained. These integral equations are converted into a matrix equation by expanding the unknown electric and magnetic surface current densities with RWG functions and using Galerkin's testing procedure is applied to convert the integral equations to a matrix equation (see, for example, Poggio & Miller, 1973; Rao et al., 1982). The singular integrals involved are evaluated with the singularity

subtraction technique available in Ylä-Oijala and Taskinen (2003) and Järvenpää et al. (2006) supplemented with high-order quadrature rules for the numerically evaluated parts.

Accurate evaluation of these integrals is important to maintain the accuracy of the solution, particularly in the near-field region. Special attention should be paid in the case of sharp corners where the field can become singular; sharp edges of a 2-D dielectric edge can induce such effects as reported, for example, in works by Dobrzynski and Maradudin (1972) and Davis (1976), suggesting that the sharp corner should be carefully treated. For the 3-D case vertices are expected to induce similar convergence issues, especially for very sharp,

lossless, and extremely subwavelength plasmonic NPs. However, our study focuses in relatively large plasmonic particles with realistic losses. A remedy to this convergence issue for the case of sharp solids, that is, Platonic solids, requires both the increase of the number of used elements (degrees of freedom) and the slight rounding of the vertices. In our study the main concern is to capture the qualitative trends of the Platonic solids; hence, we use increased number of elements but without rounding the corners, sacrificing the perfect convergence of our results; the sharp-corner effects on the convergence of the plasmonic Platonic solids will be extended in future works. Finally, once the solution to the matrix equation is available, the scattered and absorbed power can be efficiently evaluated using the surface currents and associated SIE matrices as explained by Reid and Johnson (2015).

3. Resonant Plasmonic Spectrum and Properties: Results

We start our analysis by presenting the scattering and absorption spectra, and the surface charge distributions of the two main resonances, for a sphere of volume $V=50^3 \text{ nm}^3$ corresponding to a diameter $d \approx 62.035 \text{ nm}$. Figure 2 displays the results. It is well known that a spherical Ag particle exhibits its first dipole resonance approximately at $\lambda=370 \text{ nm}$ for these size ranges (Kreibig & Vollmer, 2013). The main resonant peaks exhibit an electric dipole and quadrupole charge distribution, which is a common characteristic for the plasmonic resonances (Kreibig & Vollmer, 2013) (see insets in the figure). Note that the inset figures depict either the real or the imaginary part of the

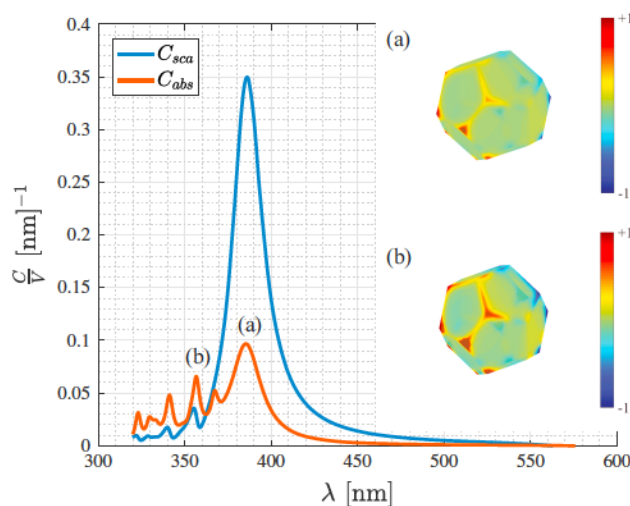


Figure 3. Volume-normalized absorption and scattering spectra for an equivolumed dodecahedron of side length $a=25.36 \text{ nm}$. The inset figures indicate the surface charge distribution for the two first absorption resonances, that is, (a) the imaginary part of charge distribution at $\lambda=385.4 \text{ nm}$ (electric dipole) and (b) the real part of the charge distribution at $\lambda=354.4 \text{ nm}$.

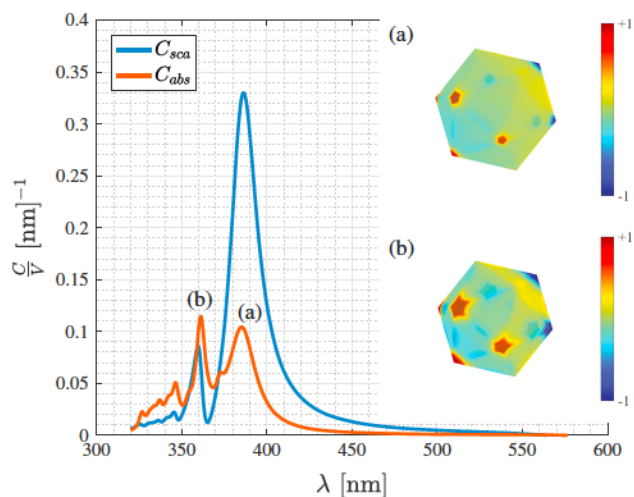


Figure 4. Volume-normalized absorption and scattering spectra for an equivolumented icosahedron of side length $a=38.55$ nm. The inset figures indicate the surface charge distribution for the two first absorption resonances, that is, (a) the imaginary part of charge distribution at $\lambda=385.8$ nm (electric dipole) and (b) the real part of the charge distribution at $\lambda=360.3$ nm.

polarization surface charges (electric flux normal to the surface). This seems to be a reasonable choice for depicting the main near-field characteristics, especially with respect to the angular distribution of the enabled resonant mode. However, a complete picture would require the presentation of both parts (Raziman & Martin, 2016). For instance, for the spherical case inset pictures in Figures 2a and 2b the strongest parts of the polarization charges are depicted, that is, imaginary part and real part of the dipole and quadrupole term, respectively. This convention is followed for every polyhedron presented hereinafter.

These results were obtained with the SIE method described above for a spherical geometry consisting of approximately 2,000 elements. The number of elements describes the number of the triangles used for the discretization of the geometry. The basis functions, used to approximate the unknown equivalent electric and magnetic surface current densities, are related to the edges of the triangular mesh, introducing in our case 6,000 degrees of freedom in the system (solid lines Figure 2). The results obtained are in extremely good agreement with the analytic Lorenz-Mie solution (dashed lines, Figure 2), readily found in classical textbooks, for example, in Bohren and Huffman (2008).

As additional special characteristics of the plasmonic sphere, Figure 2 shows the enhanced absorption values for the quadrupole resonance (Figure 2b), which is qualitatively very different from the scattering-dominated dipole regime. The variation of the balance between scattering and absorption is an

indication that dynamic effects play a significant role, thus underlining the need of a full-wave analysis. In fact, for the Platonic solids the amount of used elements is significantly higher (11,000 to 15,000 degrees of freedom). This is necessary since SIE exhibits certain convergence issues for sharp cornered plasmonic scatterers (Helsing & Perfekt, 2013; Klimov et al., 2014; Markowskei & Smith, 2017; Wallén et al., 2008).

In the following subsections we will present the main scattering characteristics of plasmonic Platonic solids. The order is with respect to increasing solid vertex angle, that is, smoother to sharper solids. The reason is that since the dodecahedron and icosahedron are intuitively closer to a sphere than a sharp tetrahedron, their spectra should also be close to that of the sphere. The sphere experiences its scattering and absorption maxima for wavelengths of $\lambda=372.7$ nm (dipole) and $\lambda=347.1$ nm (quadrupole), respectively. Note that

throughout the analysis a plane wave excitation is assumed, while C_{ext} , C_{sca} , and C_{abs} denote the extinction, scattering, and absorption cross sections, respectively (with m^2 units).

3.1. Plasmonic Dodecahedron

The smoothest of the Platonic solids, the dodecahedron, exhibits many similarities with the sphere as can be seen in its resonant scattering and absorption spectrum presented in Figure 3. Experimental studies on subwavelength regular (Kim et al., 2004; Ringe et al., 2012) and nonregular (rhombic) (Ross et al., 2015) version of this plasmonic NP suggested that the main dipole mode is affected by its plasmonic length. The plasmonic length is defined as the length between the two vertices; see, for example, Ross et al. (2015). In our case dodecahedron exhibits both the smallest length and softer vertex between all five solids.

Turning into the details, a careful comparison between Figures 2 and 3 reveals a small redshift of the main resonance peak, to approximately $\lambda=386$ nm. Higher-order modes appear in the spectrum, revealing its corner-induced scattering signature, and hence showing that even small subwavelength features have a significant impact to the overall scattering/absorption behavior.

However, these higher-order modes are not the only difference compared to the spectrum of a sphere. There is a misalignment between the scattering and

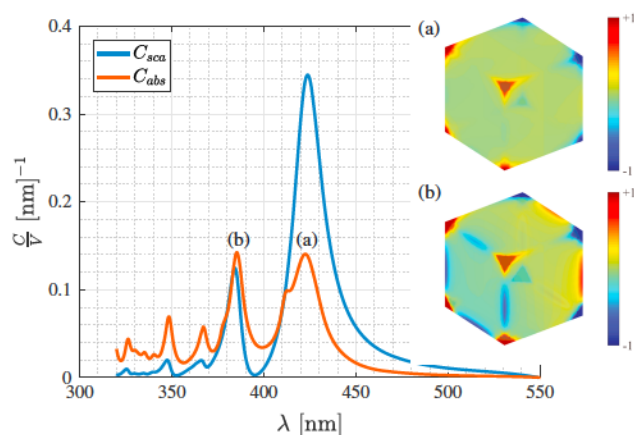


Figure 5. Volume-normalized absorption and scattering spectra for an equivolumented hexahedron (cube) with side dimension of $a=50$ nm. The inset figures indicate the surface charge distribution for the two first absorption resonances, that is, (a) the imaginary part of charge distribution at $\lambda=423.1$ nm (electric dipole) and (b) the real part of the charge distribution at $\lambda=384.7$ nm.

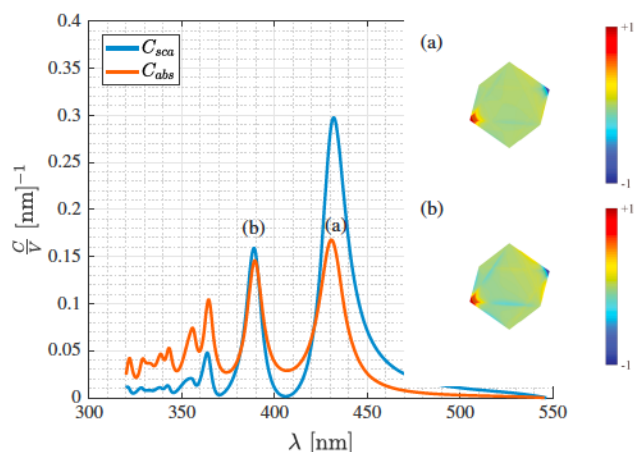


Figure 6. Volume-normalized absorption and scattering spectra for an equivolumed octahedron with side dimension $a = 64.245$ nm. The inset figures indicate the surface charge distribution for the two first absorption resonances, that is, (a) the imaginary part of charge distribution at $\lambda = 431.4$ nm (electric dipole) and (b) the real part of the charge distribution at $\lambda = 389.1$ nm.

attention to its resonant characteristics. Figure 4 gives its scattering signatures. The main dipole resonance is approximately in the same position with its equivolumed dual (dodecahedron); however, the absorption lines are enhanced. Here the same scattering/absorption resonance misalignment is observed as before. The main scattering peaks are observed at $\lambda = 385.2$ nm and $\lambda = 361.1$ nm, while the absorption maxima are at $\lambda = 386.3$ nm and $\lambda = 360.1$ nm, respectively. Finally, the two first maximum absorption charge distributions reveal a similar vertex-induced (for the dipole) and vertex-edge (for the higher modes) characteristics, as was observed for the dodecahedron.

3.3. Plasmonic Hexahedron

The hexahedron, or commonly known as cube, is the most studied geometrical shape of the whole Platonic family. Several attempts have been made for the determination of its electrostatic (polarizability) and electrodynamic response during the last 50 years. Gelder et al. (1972) and Fuchs (1974) are probably the first who studied the resonances of cubic clusters and inclusions. Indicative numerical studies (Avelin et al., 2001;

absorption maximum positions. For example, the first absorption maximum happens at $\lambda = 385.6$ nm (Figure 3a) and the second maximum at $\lambda = 356.7$ nm (Figure 3b) when the corresponding scattering peaks are $\lambda = 386$ nm and $\lambda = 355.3$ nm, respectively. The inset figures in Figure 3 reveal the charge distribution on these absorption maxima; a dipole-like behavior is visible in the first resonance and a richer charge distribution for the second one.

The main characteristic of the dipole resonance is that the charge confinement takes place on the vertices of the particle. For the second resonance, the charge confinement is extended to the edges as well. Due to this effect the categorization of this higher-order mode is a rather difficult task. Note that the above observation holds for all of the studied Platonic solids. Additionally, we observe that the sharpness of the vertex solid angle can be associated with the position of the main dipole resonances. This is an evident fact regarding the vertex-induced effects; all dipole-like distributions are mainly confined at the vertices of the Platonic solid.

3.2. Plasmonic Icosahedron

The vertex angle of the solid icosahedron is slightly sharper with respect to its dual-partner particle, the dodecahedron (see Table 1). For experimental studies of this plasmonic NP, mostly regarding its manufacturing process, see Kim et al. (2004), Ringe et al. (2012), and Keunen et al. (2014), with certain

Kim et al. (2004), Ringe et al. (2012), and Keunen et al. (2014), with certain attention to its resonant characteristics. Figure 4 gives its scattering signatures. The main dipole resonance is approximately in the same position with its equivolumed dual (dodecahedron); however, the absorption lines are enhanced. Here the same scattering/absorption resonance misalignment is observed as before. The main scattering peaks are observed at $\lambda = 385.2$ nm and $\lambda = 361.1$ nm, while the absorption maxima are at $\lambda = 386.3$ nm and $\lambda = 360.1$ nm, respectively. Finally, the two first maximum absorption charge distributions reveal a similar vertex-induced (for the dipole) and vertex-edge (for the higher modes) characteristics, as was observed for the dodecahedron.

Hohenester & Krenn, 2005; Klimov et al., 2014; Ruppin, 1996; Sihvola et al., 2004; Tzarouchis et al., 2016a, 2016b), and several experimental studies (Akselrod et al., 2014; Cortie et al., 2012; Lagos et al., 2017; Zhang et al., 2011), reveal a vibrant interest for the resonant behavior of the cube.

Figure 5 depicts the resonant spectra of the cube. The redshifted dipole mode exhibits enhanced (both in amplitude and linewidth) scattering and absorption characteristics as compared to the aforementioned solids. The sharper vertex corner ($\pi/2$) is the reason behind this redshift. In this case also the minimum scattering valley is expanded and the edge effects of the second absorption maximum are clearly observable. The main scattering resonances take place at $\lambda = 423.8$ nm and $\lambda = 384.3$ nm, with its absorption peaks shifted to $\lambda = 422.5$ nm and $\lambda = 385.3$ nm, respectively.

3.4. Plasmonic Octahedron

The octahedron, the dual shape of the cube, is a less studied particle. Its solid angle is sharper than that of the cube. Therefore, its plasmonic resonances are expected to occur for lower energies (higher wavelengths) which also can be seen in Figure 6. However, there are some differences between the responses of octahedron and cube, such as the linewidth of the resonances.

The hybrid vertex-edge mode exhibits a highly symmetric pattern with enhanced absorption peaks. Specifically, the first scattering and absorption

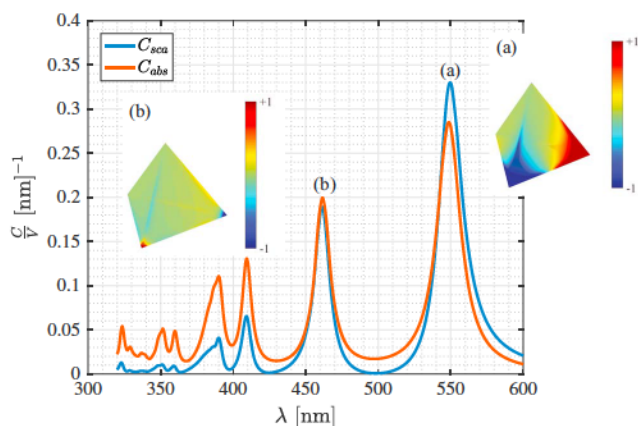


Figure 7. The volume-normalized absorption and scattering spectra of an equivolumed tetrahedron of side $a = 101.98$ nm. The inset figures indicate the surface charge distribution for the two first absorption resonances, that is, (a) the imaginary part of charge distribution at $\lambda = 549.2$ nm (electric dipole) and (b) the real part of the charge distribution at $\lambda = 461.5$ nm.

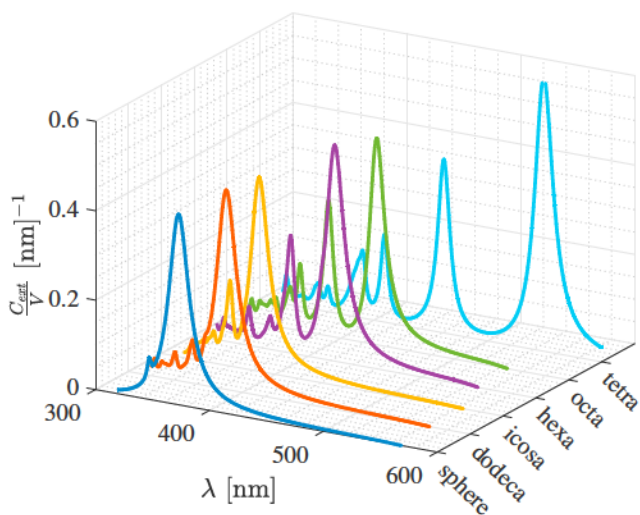


Figure 8. Comparative chart depicting the volume-normalized extinction of the five equivoled Platonic solids and the sphere. Each line corresponds to one solid.

peaks are at $\lambda = 431.9$ nm, $\lambda = 389$ nm, $\lambda = 430.7$ nm, and $\lambda = 389.4$ nm. It is interesting to observe that the minimum scattering valley is wider than that of the cube.

3.5. Plasmonic Tetrahedron

The sharpest member of Platonic solids is the tetrahedron (Kim et al., 2004), with a vertex solid angle of ≈ 0.551 and an edge length of $a = 101.98$ nm. The main dipole resonance of the tetrahedron occurs at much lower energies than for the previous solids: $\lambda = 549.7$ nm, while the second vertex-edge mode occurs at $\lambda = 461.4$ nm. Since these resonances are strongly redshifted, the relative size of the tetrahedron compared to the wavelength is much smaller than in the other Platonic NPs. This is why tetrahedron experiences enhanced absorption, as depicted in Figure 7.

Interestingly, there are two wide minimum scattering valleys around 500 nm and 425 nm. Therefore, one could say that the scattering spectrum of the tetrahedron is quantized. This kind of scattering signature might be useful for scattering tagging and low-scattering/camouflage purposes. It could be conjectured that the appearance of such scattering minima requires the existence of sharp corners in the NP.

4. Discussion and Conclusions

As an overall comparison, Figure 8 shows the extinction of all treated particles. Since the evaluated characteristics are expressed in volume-normalized quantities, a comparative chart of the extinction spectrum is meaningful. Figure 8 reveals the trends behind the scattering spectrum of the sphere and the five Platonic NPs. The development of the main scattering features, that is, the first and second resonances and scattering minima, follow the sharpness of the NPs, especially for the three last cases (tetrahedron, octahedron, and hexahedron).

In particular, the main resonant peaks of the tetrahedron, octahedron, and hexahedron occur at $\lambda_{tetra} = 549.7$ nm, $\lambda_{octa} = 430.7$ nm, and $\lambda_{hexa} = 422.5$ nm, respectively. The vertex angles are 0.551, 1.359, and $\frac{\pi}{2} \approx 1.571$, and the edge lengths are 101.98, 64.245, and 50 for the tetrahedron, octahedron, and hexahedron, respectively. The statistical correlation between the dipole absorption maximum peak and the vertices is approximately 0.988, while the wavelength-edge correlation is somewhat smaller, exhibiting roughly a value of 0.977. Due to the fact that the plasmonic resonances follow an sv-hierarchical order in terms of the lowest to highest resonant energies (lowest resonant wavelength), it stands to reason that the main plasmonic resonance is straightforwardly affected by the sharpness of the vertex.

Note that previous experimental work done by Ross et al. (2015) indicate that the edge length (plasmonic length) is the main resonant affecting mechanism. By fixing the type of solid and its volume, the edge length and vertex sharpness are mutually defined. However, in our perspective, the vertex categorization is more universal, since it is defined only by the type of solid and not its volume. This categorization follows the same philosophy as with its 2-D counterparts, where sharper corners induce resonances at lower energies, as can be found in works by Dobrzynski and Maradudin (1972), Kottmann et al. (2001), and Sturman et al. (2013).

On the other hand, earlier studies on dielectric solids, for example, in Avelin and Sihvola (2002) and Sihvola et al. (2004), revealed an hedra-hierarchical order regarding the strength of the calculated electrostatic polarizabilities. This difference can be explained by the fact that different physical mechanisms are involved for plasmonic response than in the quasistatically explainable dielectric response. In particular, sharp corners and edges facilitate the accumulation and radiation of the energy carried by the free conduction electrons, which is the main radiation enhancement mechanism behind the plasmonic resonances.

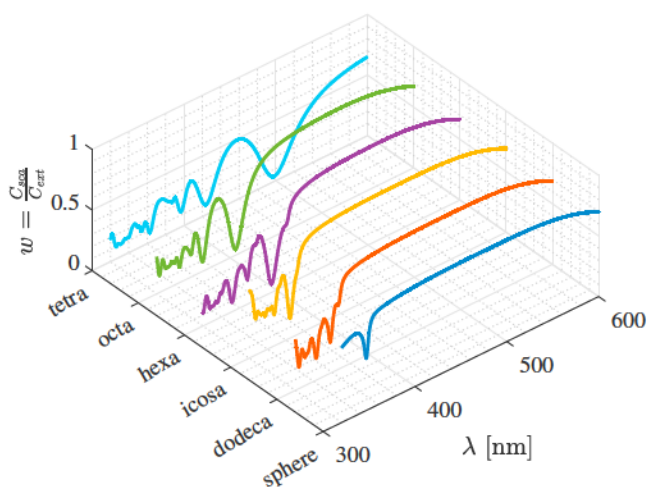


Figure 9. The scattering albedo for a sphere and the five Platonic solids. A minimum albedo can be identified for the region between the first two modes for all particles.

Another figure of merit of the qualitative characteristics of the extinction landscape is the albedo. Albedo (here denoted as w) is defined as the ratio between the scattered and the extinct total power (Tzarouchis et al., 2016b). Between the pure scattering ($w = 1$) and pure absorption ($w = 0$), it measures the composition of extinction in these two mechanisms for single or multiple NPs. For example, albedo values smaller than 0.5 indicate a dominance of the absorption mechanisms. The albedo chart in Figure 9 can be readily used for the evaluation of the scattering and absorptive characteristics for each case.

In our case almost all solids exhibit an albedo minimum valley close to their second absorptive resonance as can be seen in Figure 9. This is an indication that close to the regions of minimum scattering the absorption mechanism prevail. The most interesting case is observed for the tetrahedron since its albedo is below 0.5 almost for the entire spectrum. This can be explained again from the fact that a tetrahedron is considerably in the subwavelength region at these wavelengths, since its side is of the order $\lambda/5$ at its first dipole resonance.

As a conclusion, the resonant spectra of small regular plasmonic polyhedra have been presented. Our efforts focused on the study of the Platonic solids and their scattering characteristics. It was shown that certain features can have large impact to the scattering spectra, such as the sharpness of the corners and edges. This observation can be exploited either for design or for growth control purposes in nanotechnology applications. We estimate that this study will inspire further investigations regarding the correlation of the particular NP symmetries and the exhibited resonances. New research pathways can also include the connection of the vertex-/edge-induced effects of three-dimensional solids for both plasmonic and dielectric materials.

Acknowledgments

This work is supported by the Aalto Energy Efficiency Program (EXPECTS project) and the Aalto ELEC Doctoral School scholarship. The data presented were obtained through the implementation of the SIE method described in section 2.2 and the citations therein. The numerical data are available upon request from the corresponding author(s).

References

- Akselrod, G. M., Argyropoulos, C., Hoang, T. B., Ciraci, C., Fang, C., Huang, J., ... Mikkelsen, M. H. (2014). Probing the mechanisms of large Purcell enhancement in plasmonic nanoantennas. *Nature Photonics*, *8*(11), 835–840. <https://doi.org/10.1038/nphoton.2014.228>
- Avelin, J., & Sihvola, A. (2002). Polarizability of polyhedral dielectric scatterers. *Microwave and Optical Technology Letters*, *32*(1), 60–64. <https://doi.org/10.1002/mop.10091>
- Avelin, J., Sharma, R., Hänninen, I., & Sihvola, A. (2001). Polarizability analysis of cubical and square-shaped dielectric scatterers. *IEEE Transactions on Antennas and Propagation*, *49*(3), 451–457. <https://doi.org/10.1109/8.918620>
- Bohren, C. F., & Huffman, D. R. (2008). *Absorption and scattering of light by small particles*. New York: Wiley.
- Cortie, M. B., Liu, F., Arnold, M. D., & Niidome, Y. (2012). Multimode resonances in silver nanocuboids. *Langmuir*, *28*(24), 9103–9112. <https://doi.org/10.1021/la300407u>
- Davis, L. C. (1976). Electrostatic edge modes of a dielectric wedge. *Physical Review B*, *14*(12), 5523–5525. <https://doi.org/10.1103/PhysRevB.14.5523>
- Dobrzynski, L., & Maradudin, A. A. (1972). Electrostatic edge modes in a dielectric wedge. *Physical Review B*, *6*(10), 3810–3815. <https://doi.org/10.1103/PhysRevB.6.3810>
- Fuchs, R. (1974). Theory of the optical properties of small cubes. *Physics Letters A*, *48*(5), 353–354. [https://doi.org/10.1016/0375-9601\(74\)90463-0](https://doi.org/10.1016/0375-9601(74)90463-0)
- García de Abajo, F. J., & Howie, A. (2002). Retarded field calculation of electron energy loss in inhomogeneous dielectrics. *Physical Review B*, *65*(11), 115418. <https://doi.org/10.1103/PhysRevB.65.115418>
- Gelder, A., Holvast, J., Stoelinga, J., & Wyder, P. (1972). Localized polariton modes of small cubic crystals. *Journal of Physics C: Solid State Physics*, *5*(19), 2757–2761. <https://doi.org/10.1088/0022-3719/5/19/008>
- Grillet, N., Manchon, D., Bertorelle, F., Bonnet, C., Broyer, M., Cottancin, E., ... Pellarin, M. (2011). Plasmon coupling in silver nanocube dimers: Resonance splitting induced by edge rounding. *ACS Nano*, *5*(12), 9450–9462. <https://doi.org/10.1021/nn2041329>
- Helsing, J., & Perfekt, K. M. (2013). On the polarizability and capacitance of the cube. *Applied and Computational Harmonic Analysis*, *34*(3), 445–468. <https://doi.org/10.1016/j.acha.2012.07.006>
- Hohenester, U., & Krenn, J. (2005). Surface plasmon resonances of single and coupled metallic nanoparticles: A boundary integral method approach. *Physical Review B*, *72*(19), 195429.
- Järvenpää, S., Taskinen, M., & Ylä-Oijala, P. (2006). Singularity subtraction technique for high-order polynomial vector basis functions on planar triangles. *IEEE Transactions on Antennas and Propagation*, *54*(1), 42–49.
- Johnson, P. B., & Christy, R.-W. (1972). Optical constants of the noble metals. *Physical Review B*, *6*(12), 4370.
- Kern, A. M., & Martin, O. J. (2009). Surface integral formulation for 3D simulations of plasmonic and high permittivity nanostructures. *Journal of the Optical Society of America. A*, *26*(4), 732–740.
- Keunen, R., Cathcart, N., & Kitaev, V. (2014). Plasmon mediated shape and size selective synthesis of icosahedral silver nanoparticles via oxidative etching and their 1-D transformation to pentagonal pins. *Nanoscale*, *6*(14), 8045–8051. <https://doi.org/10.1039/c4nr01477d>
- Kim, F., Connor, S., Song, H., Kuykendall, T., & Yang, P. (2004). Platonic gold nanocrystals. *Angewandte Chemie*, *116*(28), 3759–3763. <https://doi.org/10.1002/ange.200454216>
- Klimov, V., Guo, G. Y., & Pikhota, M. (2014). Plasmon resonances in metal nanoparticles with sharp edges and vertices: A material independent approach. *The Journal of Physical Chemistry C*, *118*(24), 13,052–13,058. <https://doi.org/10.1021/jp412349f>
- Kottmann, J. P., Martin, O. J. F., Smith, D. R., & Schultz, S. (2001). Plasmon resonances of silver nanowires with a nonregular cross section. *Physical Review B*, *64*(23), 235402. <https://doi.org/10.1103/PhysRevB.64.235402>
- Kreibig, U. (1974). Electronic properties of small silver particles: The optical constants and their temperature dependence. *Journal of Physics F: Metal Physics*, *4*(7), 999–1014. <https://doi.org/10.1088/0305-4608/4/7/007>
- Kreibig, U., & Vollmer, M. (2013). *Optical properties of metal clusters* (Vol. 25). Berlin: Springer Series in Material Science.
- Lagos, M. J., Trügler, A., Hohenester, U., & Batson, P. E. (2017). Mapping vibrational surface and bulk modes in a single nanocube. *Nature*, *543*(7646), 529–532. <https://doi.org/10.1038/nature21699>

- Markowski, A. J., & Smith, P. D. (2017). Measuring the effect of rounding the corners of scattering structures. *Radio Science*, 52, 693–708. <https://doi.org/10.1002/2017RS006276>
- Mitche, S., Marguet, S., Charra, F., & Douillard, L. (2017). Near-field localization of single Au cubes: A group theory description. *The Journal of Physical Chemistry C*, 121, 4517–4523. <https://doi.org/10.1021/acs.jpcc.6b10585>
- Noguez, C. (2007). Surface plasmons on metal nanoparticles: The influence of shape and physical environment. *Journal of Physical Chemistry C*, 111(10), 3606–3619. <https://doi.org/10.1021/jp066539m>
- Palik, E. D. (1998). *Handbook of optical constants of solids* (Vol. 3). London: Academic Press.
- Poggio, A. J., & Miller, E. K. (1973). Integral equation solutions of three-dimensional scattering problems. In R. Mittra (Ed.), *Computer Techniques for Electromagnetics*. Oxford: Pergamon Press.
- Quinten, M. (2010). *Optical properties of nanoparticle systems: Mie and beyond*. Weinheim: Wiley-VCH.
- Rao, S. M., Wilton, D. R., & Glisson, A. W. (1982). Electromagnetic scattering by surfaces of arbitrary shape. *IEEE Transactions on Antennas and Propagation*, 30(3), 409–418. <https://doi.org/10.1109/TAP.1982.1142818>
- Raziman, T. V., & Martin, O. J. F. (2016). Does the real part contain all the physical information? *Journal of Optics*, 18(9), 95002. <https://doi.org/10.1088/2040-8978/18/9/095002>
- Reid, M. T. H., & Johnson, S. G. (2015). Efficient computation of power, force, and torque in BEM scattering calculations. *IEEE Transactions on Antennas and Propagation*, 63(8), 3588–3598. <https://doi.org/10.1109/TAP.2015.2438393>
- Ringe, E., Langille, M. R., Sohn, K., Zhang, J., Huang, J., Mirkin, C. A., ... Marks, L. D. (2012). Plasmon length: A universal parameter to describe size effects in gold nanoparticles. *The Journal of Physical Chemistry Letters*, 3(11), 1479–1483. <https://doi.org/10.1021/jz300426p>
- Ross, M. B., Ku, J. C., Vaccarella, V. M., Schatz, G. C., & Mirkin, C. A. (2015). Nanoscale form dictates mesoscale function in plasmonic DNA—Nanoparticle superlattices. *Nature Nanotechnology*, 10(5), 453–458. <https://doi.org/10.1038/nnano.2015.68>
- Ruppin, R. (1996). Plasmon frequencies of cube shaped metal clusters. *Zeitschrift für Physik D Atoms, Molecules and Clusters*, 36(1), 69–71. <https://doi.org/10.1007/BF01437423>
- Sihvola, A., Ylä-Oijala, P., Järvenpää, S., & Avelin, J. (2004). Polarizabilities of platonic solids. *IEEE Transactions on Antennas and Propagation*, 52(9), 2226–2233. <https://doi.org/10.1109/TAP.2004.834081>
- Solis, D. M., Taboada, J. M., Landesa, L., Rodríguez, J. L., & Obelleiro, F. (2015). Squeezing Maxwell's equations into the nanoscale. *Progress In Electromagnetics Research*, 154, 35–50.
- Sturman, B., Podivilov, E., & Gorkunov, M. (2013). Universal plasmonic properties of two-dimensional nanoparticles possessing sharp corners. *Physical Review B*, 87(11), 115406. <https://doi.org/10.1103/PhysRevB.87.115406>
- Taboada, J. M., Rivero, J., Obelleiro, F., Araújo, M. G., & Landesa, L. (2011). Method-of-moments formulation for the analysis of plasmonic nano-optical antennas. *Journal of the Optical Society of America. A*, 28(7), 1341–1348.
- Tzarouchis, D. C., Ylä-Oijala, P., & Sihvola, A. (2016). Plasmonic modes on rounded hexahedral and octahedral nano-antennas. In *2016 URSI International Symposium on Electromagnetic Theory (EMTS)*, IEEE, Espoo, Finland, pp. 767–770. <https://doi.org/10.1109/URSI-EMTS.2016.7571514>
- Tzarouchis, D. C., Ylä-Oijala, P., Ala-Nissila, T., & Sihvola, A. (2016a). Plasmonic properties and energy flow in rounded hexahedral and octahedral nanoparticles. *Journal of the Optical Society of America. B*, 33(12), 2626–2633. <https://doi.org/10.1364/JOSAB.33.002626>
- Tzarouchis, D. C., Ylä-Oijala, P., Ala-Nissila, T., & Sihvola, A. (2016b). Shape effects on surface plasmons in spherical, cubic, and rod-shaped silver nanoparticles. *Applied Physics A*, 122(4), 298. <https://doi.org/10.1007/s00339-016-9851-y>
- Varti, O. S., Ylä-Oijala, P., Markkanen, J., Puupponen, S., Seppälä, A., Sihvola, A., & Ala-Nissila, T. (2016). On the applicability of discrete dipole approximation for plasmonic particles. *Journal of Quantitative Spectroscopy and Radiation Transfer*, 169, 23–35. <https://doi.org/10.1016/j.jqsrt.2015.10.003>
- Wallén, H., Kettunen, H., & Sihvola, A. (2008). Surface modes of negative-parameter interfaces and the importance of rounding sharp corners. *Metamaterials*, 2(2–3), 113–121. <https://doi.org/10.1016/j.metmat.2008.07.005>
- Wallén, H., Kettunen, H., & Sihvola, A. (2009). Composite near-field superlens design using mixing formulas and simulations. *Metamaterials*, 3(3–4), 129–139. <https://doi.org/10.1016/j.metmat.2009.08.002>
- Weyl, H. (2015). *Symmetry*. Princeton, NJ: Princeton University Press.
- Yang, Y., Miller, O. D., Christensen, T., Joannopoulos, J. D., & Soljačić, M. (2017). Low-loss plasmonic dielectric nanoresonators. *Nano Letters*, 17(5), 3238–3245. <https://doi.org/10.1021/acs.nanolett.7b00852>
- Ylä-Oijala, P., & Taskinen, M. (2003). Calculation of CFIE impedance matrix elements with RWG and $n \times$ RWG functions. *IEEE Transactions on Antennas and Propagation*, 51(8), 1837–1846.
- Ylä-Oijala, P., Taskinen, M., & Sarvas, J. (2005). Surface integral equation method for general composite metallic and dielectric structures with junctions. *Progress In Electromagnetics Research*, 52, 81–108.
- Ylä-Oijala, P., Markkanen, J., Järvenpää, S., & Kiminki, S. P. (2014). Surface and volume integral equation methods for time-harmonic solutions of Maxwell's equations. *Progress In Electromagnetics Research*, 149, 15–44.
- Zhang, S., Bao, K., Halas, N. J., Xu, H., & Nordlander, P. (2011). Substrate-induced Fano resonances of a plasmonic nanocube: A route to increased-sensitivity localized surface plasmon resonance sensors revealed. *Nano Letters*, 11(4), 1657–1663. <https://doi.org/10.1021/nl200135r>